Turkish Journal of Electrical Engineering & Computer Sciences

http://journals.tubitak.gov.tr/elektrik/

Research Article

Turk J Elec Eng & Comp Sci
(2017) 25: 950 – 964

doi:10.3906/elk-1507-80

A novel wound field flux switching machine with salient pole rotor and nonoverlapping windings

Faisal KHAN*, Erwan SULAIMAN, Md. Zarafi AHMAD
Research Center for Applied Electromagnetics, Universiti Tun Hussein Onn Malaysia, Batu Pahat, Johor, Malaysia

Received: 09.07.2015 • **Accepted/Published Online:** 10.03.2016 • **Final Version:** 10.04.2017

Abstract: A flux switching machine (FSM) with a segmented rotor and nonoverlapping windings is an attractive alternative for driving high torque density applications. However, a rotor with segments makes the motor less robust as well as difficult to be assembled, while a FSM with salient rotor and overlapping windings inherits high copper losses and less efficiency due to high coil volume. In this paper, a novel structure of FSM with nonoverlapping windings and salient rotor is proposed, making it different from the 10Slot-8Pole segmental and salient rotor FSM. Several design parameters defined in the rotor, armature coil, and field excitation coil are treated by the deterministic optimization approach until the target values are achieved and the performances are analyzed by two-dimensional finite element analysis. The optimized design has achieved average torque of 27.06 Nm and power of 6.83 kW at armature current density, J_a, of 30 A_{rms}/mm^2 and maximum field current density, J_e, of 30 A/mm^2, which is greater than the 10Slot-8Pole segmental rotor and salient rotor FSM. Wound field FSMs with salient rotor and nonoverlapping windings should be considered as promising candidates for hybrid electric vehicles and all-electric boats due to their high torque density, robust rotor, and fewer losses.

Key words: Flux switching motor, salient rotor, nonoverlapping windings, optimization, torque, power

1. Introduction

Concerns regarding the relatively high cost and potential resource issues of permanent magnet (PM) excited machines are driving various efforts to consider machines with fewer or no PMs. Conventional electric machines, including induction machines, switched reluctance machines, and wound field synchronous machines, are potential competitors for substitution of PM excited machines. Induction machines have advanced control strategies, are cost-effective, and require low maintenance. Nonetheless, the efficiency and torque/power density are less than in the PM excited machines [1]. Switched reluctance machines exhibit large torque pulsation and high acoustic noise. As for the conventional wound field synchronous machine, it is a non-PM machine recognized to have less losses, to avoid the demagnetization issue of PMs, and to be of low cost. However, in these machines, slip-rings/brushes are normally required to supply DC power to the rotor [2].

Flux switching machines (FSMs) are a new class of brushless electric machines. Over the last decade many novel and new FSM topologies have been developed for various applications, including automotive [3], home appliance [4], and aerospace [5] applications. FSMs combine the advantages of the high torque density of synchronous machines and the robust rotor structure of switched reluctance motors by placing a PM and/or windings in the stator [6,7]. High torque density and high efficiency has dominated the research on FSMs by

*Correspondence: faisalkhan@ciit.net.pk

using PMs for primary excitation. However, their application is limited by the high cost of rare earth magnet material, i.e. NdFeB, and working environmental temperature. Additionally, it is difficult to operate the PM FSM at high speed in flux-weakening regions due to fixed PM excitation. In order to reduce the cost, one of the possible solutions is to replace the PM with a field excitation coil (FEC). For this reason, some wound field FSMs are proposed for low-cost applications [8–10]. The wound field FSM is a novel brushless machine having windings located in the stator [11], having advantages of a magnet-less machine, simple construction, low cost, and variable flux control capabilities suitable for various applications when compared with other FSMs.

With these advantages, a 24S-10P three-phase wound field salient rotor FSM has been developed from a 24S-10P PM FSM in which the PM is replaced by the FEC [12]. The total flux generation is limited because of adjacent DC FEC isolation and thus machine performance is affected. To overcome the drawbacks, new structures of 24S-10P and 24S-14P wound field salient rotor with single DC polarity have been introduced [13]. Although less leakage flux and much simpler design of a single DC FEC are the advantages of the proposed machine, the overlapping armature and field windings, which increase the cost and copper losses, thus reducing the efficiency, need to be overcome. A toothed-rotor structure with overlapping windings is used to produce bipolar flux linkages with high torque, but the problem of high copper losses remains to be resolved [14].

In recent research, the performance analysis of FSMs is improved by means of segmental rotor design [15]. Nonoverlapping windings and segmental rotors were used in [16] to enhance the efficiency by lessening the copper losses. However, this machine cannot be employed for high speed applications due to less robust rotor structure. Figures 1a and 1b illustrate a wound field salient rotor FSM with overlapping windings (OWFSal FSM) and wound field segmental rotor FSM with nonoverlapping windings (NWFSeg FSM) at the stator, respectively. The concept of overlapping and nonoverlapping windings is shown using elementary rectilinear structures of stator. In the OWFSal FSM, the armature and field windings are wound around two stator poles overlapping each other, while in NWFSeg FSM, armature and field windings are wound around each pole separately and hence are not overlapping each other. A single-phase wound field FSM was thoroughly examined in [17–19]. In that machine, both armature and field windings are entirely pitched and therefore the end-winding is longer. Two single phase wound field salient rotor FSM topologies with armature and DC FEC having different coil-pitches of 1 and 3 slot-pitches and having the same coil-pitch of 2 slot-pitches respectively were discussed in [20]. Accordingly, the iron loss was reduced, thus boosting the efficiency, but the problems of overlapping windings and less efficiency are unsuited for practicality.

In this paper, a novel structure of a wound field salient rotor FSM with nonoverlapping windings (NWFSal FSM) having 12 stator poles and 10 rotor poles is presented and analyzed. JMAG designer ver. 13 is used to develop the structure and is validated by the results obtained by 2D-FEA. Since the initial design of the machine fails to achieve target torque and power, compared with 10Slot-8Pole segmental and salient rotor FSMs, the performances are improved by optimization of numerous design parameters defined in the rotor, FEC, and armature slot area.

2. Initial design specifications of wound field FSMs

The selected sizing of the NWFSal FSM, following the geometry of Figure 2, is summarized with the parameters shown in Table 1. The selection of initial dimensions is based on the following assumptions: armature coil slot area and the FEC slot area are set to be trapezoidal shape with same slot area; the initial rotor radius chosen is in the region of 60% to 70% of whole machine radius. The number of FEC and armature turns is calculated by using Eq. (1):

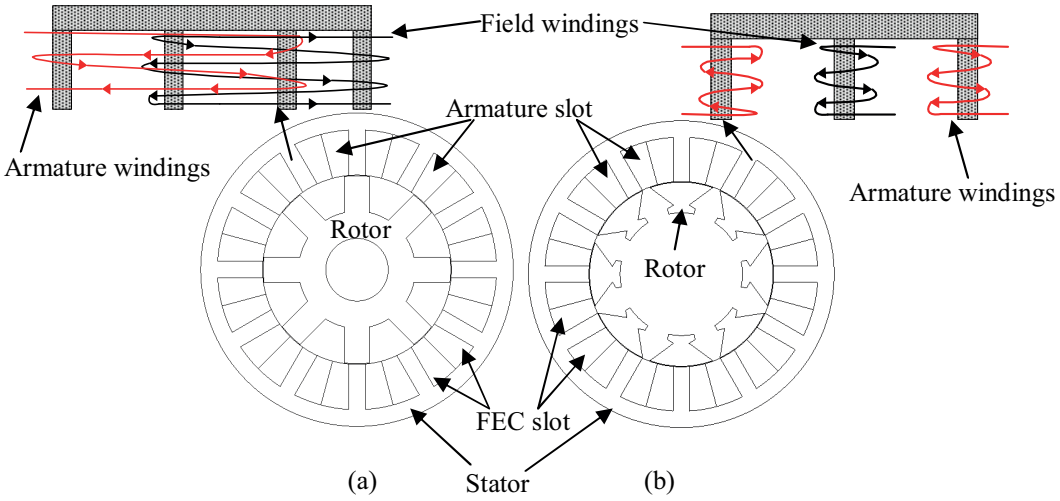

Figure 1. (a) 12Slot-8Pole OWFSal FSM; (b) 12Slot-8Pole NWFSeg FSM.

$$N = \frac{J\alpha S}{I}, \tag{1}$$

where N, J, α, S, and I are number of turns, current density, filling factor, slot area, and input current, respectively.

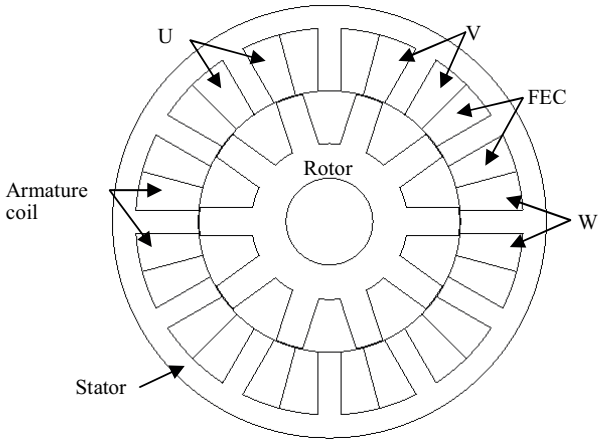

Figure 2. Initial design of the 12Slot-10Pole NWFSal FSM.

The dimensions of existing FSMs and the proposed 12Slot-10Pole NWFSal FSM are kept the same for a fair comparison. All the wound field FSMs are simulated using JMAG designer ver. 13 for comparison of their various characteristics such as flux linkage, cogging torque, average torque, and power.

3. Mathematical model of wound field FSM

The wound field FSM can be modeled using the general theory of synchronous machines to verify the original method of calculation. In a wound field synchronous motor, the field winding is mounted on the rotor and the armature winding is located in the stator, while in wound field FSM, both armature and field windings are located in the stator. The wound field FSM completes two electrical cycles per revolution as opposed to the

one by the synchronous machine. For a general AC wound field synchronous machine with a rotating field, the three-phase voltages, $V_{3\phi f}$, are given in terms of the phase current $i_{3\phi f}$ by

$$V_{3\varphi f} = Ri_{3\varphi f} + \frac{d}{dt}\left(\psi_{3\varphi f}\right), \tag{2}$$

where ψ is the flux linkage and R is the resistance per phase.

Table 1. Initial geometric parameters of design.

Parameters	Values
Radius of stator [mm]	75
Radius of rotor [mm]	45
Length of air gap [mm]	0.3
Stator pole width [mm]	8
Rotor pole width [mm]	9.6
Armature slot area [mm^2]	232.11
FEC slot area [mm^2]	232.11
FEC current [A]	79.13
Armature current [A]	111.90
No. of turns of FEC	44
No. of turns of armature coil	44
Filling factor	0.5
Stack length [mm]	70

As the flux linkage of the wound field FSM changes with rotor position, the inductance is considered to be dependent on rotor position, θ_r.

$$\psi_{3\varphi f} = L_{3\varphi f}\left(i_{3\varphi}, i_f, \theta_r\right) i_{3\varphi f} \tag{3}$$

Here, $L_{3\phi f}$ is the matrix of self-inductance and mutual inductance of the FEC and armature coil of the wound field FSM.

The torque developed by the FSM is proportional to FEC current, i_f, and armature coil current, i_a, as stated in [21] and given by:

$$T = i_a i_f \frac{dM_{fa}}{dt}, \tag{4}$$

where M_{fa} is the mutual inductance of the armature coil and FEC. The excitation torque will be produced by the interaction of the FEC and armature phase coil through their mutual inductances. The self-inductances of armature and field windings are independent of rotor position and therefore constant. For simplification purposes of torque, half of the machine is considered and it is assumed that the field coil only interacts with the adjacent armature coil because they are arranged in alternate sequence, as can be seen in Figure 2.

$$\begin{aligned} T \;=\; & 2(i_{f1} i_{aU} \tfrac{dM_{f1-aU}}{d\theta} + i_{f1} i_{aW} \tfrac{dM_{f1-aW}}{d\theta}) \\ & +2(i_{f2} i_{aU} \tfrac{dM_{f2-aU}}{d\theta} + i_{f2} i_{aV} \tfrac{dM_{f2-aV}}{d\theta}) \\ & +2(i_{f3} i_{aV} \tfrac{dM_{f3-aV}}{d\theta} + i_{f3} i_{aW} \tfrac{dM_{f3-aW}}{d\theta}) \end{aligned} \tag{5}$$

Here, the subscripts U, V, and W represent the three phases of the armature coil.

4. Performance analysis of initial design based on 2D-FEA

4.1. Flux linkage and cogging torque

The flux produced by the FEC at maximum field current density J_e of 30 A/mm^2 is illustrated in Figure 3. The flux linkage of the NWFSeg FSM is high due to the short flux path when compared to the OWFSal FSM and NWFSal FSM, respectively. Moreover, the proposed design has flux leakage to the surrounding core and a long flux path, and flux does not flow through all stator teeth, which creates a problem of less torque generation. From Figure 4, it is obvious that the NWFSeg FSM has high flux magnitude of 0.04 Wb while the NWFSal FSM has much less flux magnitude. To utilize the flux completely in the proposed design, optimization of various machine parameters is adopted to enhance the flux linkage from stator to rotor and back to stator.

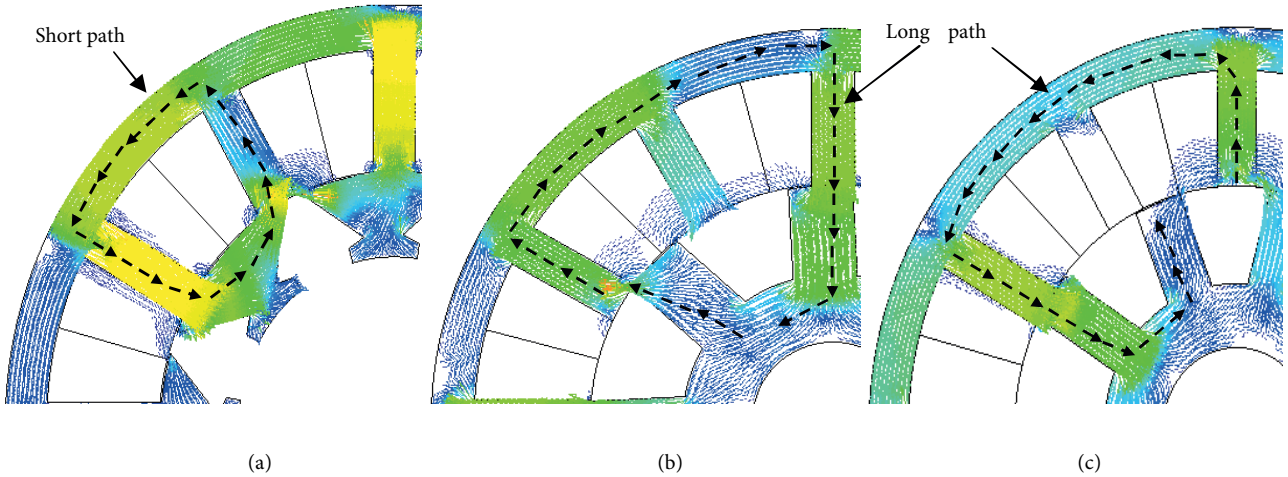

Figure 3. Flux distribution of (a) NWFSeg FSM, (b) OWFSal FSM, (c) NWFSal FSM.

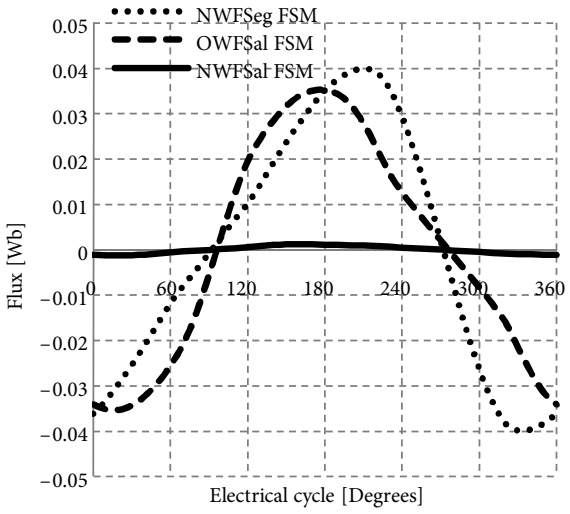

Figure 4. Flux linkage of wound field FSMs.

Cogging torque values, as illustrated in Figure 5, do not add to the electromagnetic output torque, only to effects in torque pulsations, which correspond to undesirable vibration and acoustic noise. Cogging torque

has been the subject of recent investigations in the pursuit of methods of minimizing torque ripple in various configurations of electrical machines. Cogging torque, T_{cog}, may be described by a general Fourier series expansion for the wound field FSMs employed as:

$$T_{cog}(\theta_r) = \sum_{h=1}^{\infty} T_h Sin(hN_{st}\theta_r + \varphi_h), \tag{6}$$

where N_{st} is the number of stator teeth, and T_h and ϕ_h are the Fourier coefficients for the harmonic cogging torque magnitude and phase, respectively. The OWFSal FSM has high peak to peak cogging torque of 46 Nm while the NWFSeg and NWFSal FSMs have peak to peak cogging torque of 8 Nm and 10 Nm at maximum field current density J_e of 30 A/mm^2.

4.2. Torque vs. armature current density at maximum field current density

The torque versus armature current density J_a characteristics of wound field FSMs at maximum field current densities, J_e, of 30 A/mm^2 are plotted in Figure 6. The electromagnetic torque, T_e, developed in an electrical machine generally consists of a reluctance torque component, T_{rel}, and an excitation torque component, T_{exc}, and may be expressed in a polyphase arrangement as [16]:

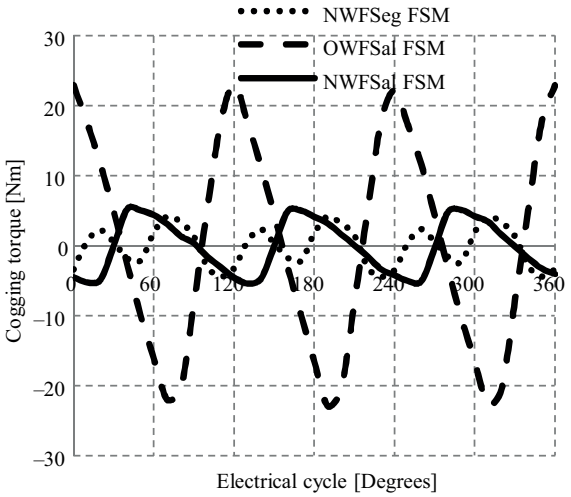

Figure 5. Cogging torque of wound field FSMs.

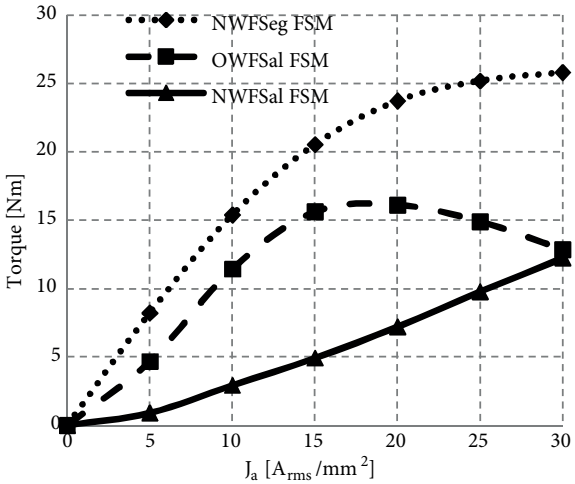

Figure 6. Torque vs. J_a at J_e of 30 A/mm^2.

$$T_e = \sum_k T_{rel,k} + \sum_k T_{exc,k}, \tag{7}$$

$$T_e = \frac{1}{2}\sum_k i_k^2 \frac{dL_k}{d\theta} + \sum_k i_k \frac{d\psi_{exc}}{d\theta}, \tag{8}$$

where L_k is the phase winding inductance, ψ_{exc} is the flux linkage due to field excitation, i_k is the phase current, θ is the electrical angular position of the rotor, and k = a, b, c is the phase designation. As the operation of the FSM with sinusoidal current is with the current placed in phase with the back-EMF, the

principal torque is due to T_{exc} and the contribution of T_{rel} is negligible, and so T_e can be expressed as:

$$T_e = \frac{P_i(t)}{\omega_r} = \frac{\sum_k e_k(t) i_k(t)}{\omega_r} \approx \sum_k T_{exc,k}, \tag{9}$$

with P_i being the instantaneous power, ω_r the rotational speed, and e_k the phase back-EMF. The flexible characteristic of the average torque, controllable by both the field and armature current, is one of the major advantages of NWFSal FSMs.

The maximum torque of 25.80 Nm is obtained by the NWFSeg FSM at maximum J_e and J_a of 30 $\mathrm{A/mm^2}$, which is approximately two times greater than the other designs. Although the flux produced by the overlapping windings arrangement is high in the OWFSal FSM, torque generation is limited because most of the FEC and armature coil flux cancel the effect of each other instead of adding up while no such phenomenon is observed in NWFSeg and NWFSal FSMs. It can be seen from the figure that when the value of J_a is increased beyond 20 $\mathrm{A}_{rms}/\mathrm{mm^2}$, the torque performance is slightly reduced. This occurs due to excessive armature coil flux that generates negative torque, thus reducing the performance. The average torque of the NWFSal FSM increases linearly with increasing J_a, but nevertheless it has less value compared to the NWFSeg FSM due to less flux linkage.

4.3. Power vs. armature current density at maximum field current density

At maximum J_a and J_e of 30 $\mathrm{A/mm^2}$, the power achieved by the NWFSeg FSM is 6.5 kW, which is 46% and 76% higher than the NWFSal and OWFSal FSMs, respectively, as illustrated in Figure 7. The power of the proposed design increases linearly with J_a, affirming less copper losses, while for the other designs continuous decrement of power is observed at certain values of J_a due to high copper losses at high armature current. The proposed 12Slot-10Pole NWFSal FSM has achieved less power, which can be further enhanced by optimization.

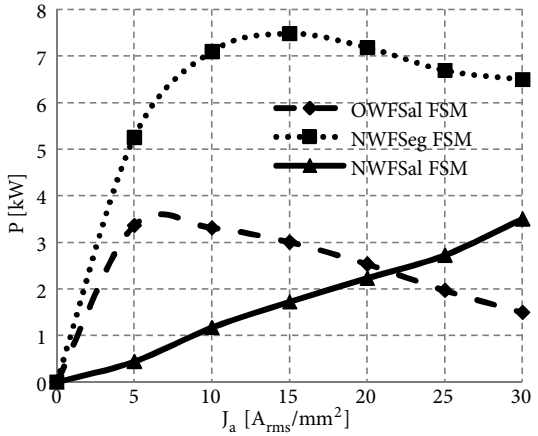

Figure 7. Power vs. J_a at J_e of 30 $\mathrm{A}_{rms}/\mathrm{mm^2}$.

5. Procedures for optimization of design and analysis

The performance analyses of the initial structure of the 12Slot-10Pole NWFSal FSM are examined. The initial torque and power obtained are 12.23 Nm and 3.12 kW at a maximum speed of 2438 rpm, which is far from the target requirements. In order to accomplish better characteristics, design free parameters A_1 to A_7 are defined

in the stator and rotor part, as illustrated in Figure 8a. By keeping the air gap constant and adjusting design free parameters A_1 to A_7 using a deterministic optimization approach, the maximum performance of the NWFSal FSM will be achieved. The first step is to change the rotor radius, A_1, which is the dominant design parameter and torque increases with increase in rotor radius, while keeping other parameters constant. Then, keeping A_1 at maximum value, the rotor pole width A_2 and rotor pole depth A_3 are adjusted. Once a combination of promising parameters A_1, A_2, and A_3 for highest torque is determined, the second step is done by changing the armature slot parameters A_4 and A_5 while keeping the rotor parameters and FEC slot area constant. Finally, the FEC slot area is updated by keeping the other parameters constant. To achieve the maximum torque and power, the design procedure above is conducted repeatedly by changing A_1 to A_7, gradually. Figure 8b illustrates two cycles of optimization to achieve high torque by updating various parameters. From Figure 8b, it is obvious that the torque first increases to a certain level by adjusting the parameters of the machine and then becomes constant, affirming the optimized parameters of the proposed machine. During cycle 1, an increment of 36% in torque value is attained by updating the dominant rotor parameter, A_1, while A_2, A_3, A_4, and A_5 have slightly enhanced the torque. For armature slot, the value of width parameter A_4 actually decreases from initial value, leaving a vacant space to increase the width of the stator pole and thus increasing the flux linkage to rotor. For the FEC slot, the updated parameters A_6 and A_7 have increased the torque up to 21%. As the slot area decreases, the FEC utilizes maximum flux to generate more torque compared to the initial design. Additionally, more space is available at the stator yolk for the smooth flow of flux to the rotor. After completion of cycle 2, much less increment of torque, approximately 0.5 Nm, is observed. It can be concluded from the discussion that variations of rotor radius and FEC slot parameters play a vital role in maximum torque production. The refined structure of this machine, which produced the maximum power and torque, is shown in Figure 9, while comparisons between the initial and refined design parameters are listed in Table 2.

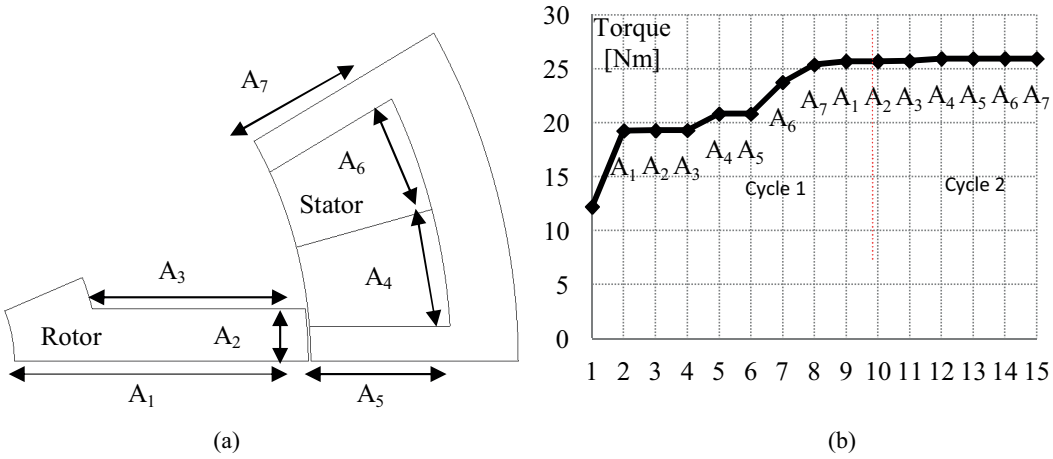

Figure 8. Deterministic optimization: (a) design parameters of 12Slot-10Pole NWFSal FSM; (b) effect of various motor parameters on average torque.

5.1. Influence of design parameters on flux distribution

The flux produced by the FEC at maximum field current density J_e of 30 A/mm^2 is illustrated in Figures 10a and 10b. It can be seen that, after optimization, the effect of leakage flux is reduced and flux flows through the stator pole when compared to the initial design, indicated by black circles. As a result, less cogging torque

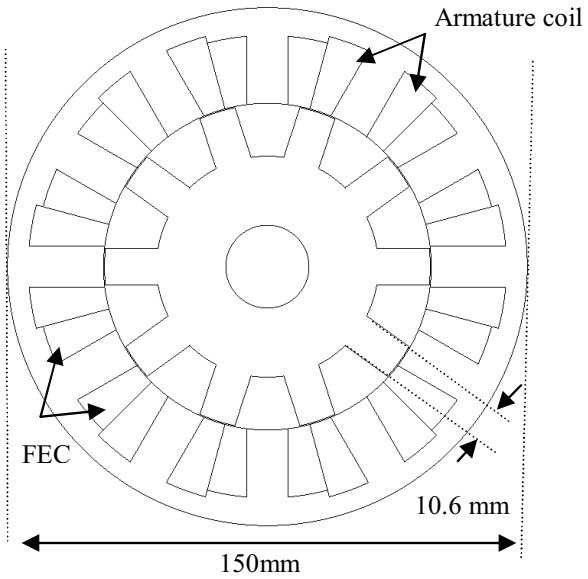

Figure 9. Refined design of 12Slot-10Pole NWFSal FSM.

Table 2. Initial and refined design parameters.

	Parameters	Initial	Improved
A_1	Radius of rotor [mm]	45	47
A_2	Width of rotor [mm]	9.6	10.6
A_3	Depth of rotor [mm]	21	16
A_4	Armature coil slot width [mm]	13	11
A_5	Armature coil slot depth [mm]	21.7	21.7
A_6	FEC slot width [mm]	13	11
A_7	FEC slot depth [mm]	21.7	19.7
A_g	Length of air gap [mm]	0.3	0.3
S_a	Armature coil slot area [mm^2]	232.11	199.91
S_{fec}	FEC slot area [mm^2]	232.11	176.32
T	Average torque [Nm]	12.23	25.95
P	Power [kW]	3.12	4.97

and back-EMF less than the applied voltage at open circuit condition under maximum speed operation are produced, which minimizes the vibrations and makes it easy to protect the switching devices when the inverter is switched off due to some malfunctions. Moreover, iron loss is also reduced, which helps the machine to be more efficient. In Figure 10b, the flux strength at the stator is increased, the flux path is reduced, and a large amount of fluxes flow to the rotor side, resulting in maximum torque production. The magnetic field density of the refined design is uniformly distributed and the stator and rotor core promise much higher flux linkage. As an example, flux of 1.6 T is obtained at the outer stator yoke, which is 53% higher than in the initial design.

5.2. Torque and power versus speed characteristics

The torque and power versus speed curves of the initial and refined design of the 12Slot-10Pole NWFSal FSM are plotted in Figure 11. Maximum torque of 12.24 Nm and 25.95 Nm is obtained at the base speed of 2263 rpm and 1831 rpm, and the torque of the machine decreases if operated beyond the base speed. The power

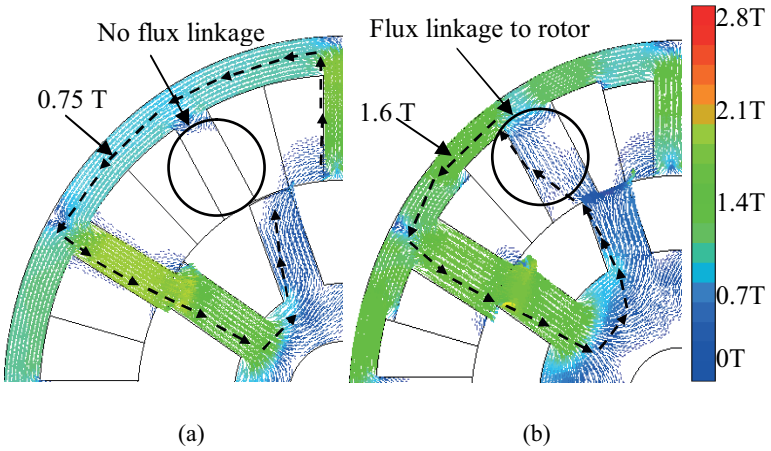

Figure 10. Flux distribution of (a) initial design and (b) refined design.

starts to decrease until 3.2 kW beyond the base speed due to increase in iron loss while at maximum torque; the power achieved by the refined design is 4.97 kW at a base speed of 1831 rpm. The proposed machine has achieved high torque and power when compared with the 12Slot-8Pole OWFSal FSM. Although the power of the refined machine is less than that of the segmental rotor FSM, robust rotor structure and almost equal torque production improve its ability to be applied in high speed applications.

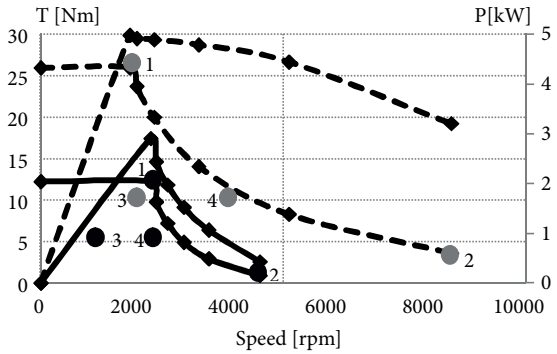

Figure 11. Comparison of torque/power versus speed characteristics of initial and refined design.

5.3. Motor losses and efficiency analyses

The motor copper losses in the armature coil and FECs, iron losses in all laminated cores, and efficiency are computed by 2D-FEA. The formula used to calculate the copper losses is as follows:

$$P_c = \rho(2L + 2L_{end}) \times J \times I \times N \times N_{slot}, \tag{10}$$

where P_c, L, and L_{end} are copper loss, stack length, and estimated end coil length, respectively, while J, I, N, and N_{slot} are current, current density, number of turns, and number of slots and ρ is copper resistivity, having a constant value of $2.224 \times 10^{-8}\,\Omega$m.

The copper losses, iron losses, and efficiency of the initial and refined designs of the NWFSal FSM at maximum torque, maximum power, and frequent operating point under light load driving situation, noted as No. 1 to No. 4, are shown in Figures 12a and 12b, where P_i is the iron losses and P_{out} is the output power. At maximum torque operating point No. 1, the efficiencies of the initial and refined designs are slightly degraded

due to high copper losses, while at operating point No. 2, the effect of iron loss also increases at high speed, which further degrades the efficiency of the initial design. After following various steps of optimization, the effect of iron losses and copper losses for the refined design is reduced, as can be seen from Figure 12b, which further improves the efficiency. Furthermore, at operating points No. 3 and No. 4, the refined machine achieves comparatively high average efficiency of approximately 73% compared with the initial average efficiency of 61%. The copper losses can be further minimized by improving the motor winding packing factor and number of turns analysis. In this way, the motor efficiency can surpass 73% to further improve the proposed 12Slot-10Pole NWFSal FSM as a potential candidate for high speed applications.

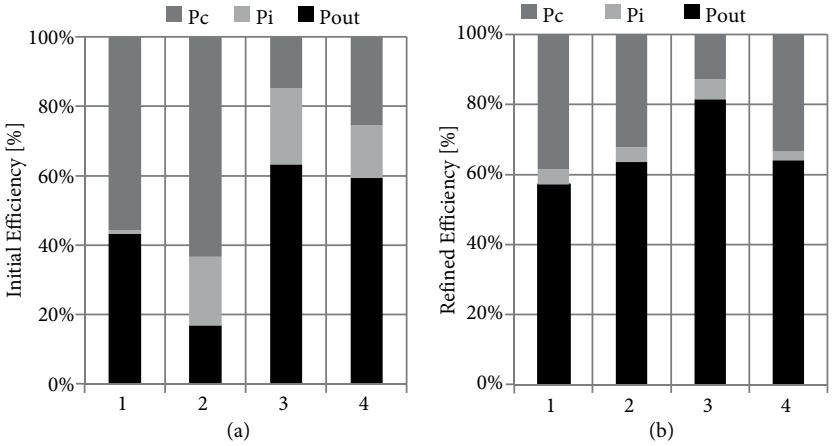

Figure 12. Losses and efficiency of the (a) initially designed and (b) refined design motor over operating points given in Figure 11.

6. Transformation of trapezoidal slot to rectangular slot

The refined design of the 12Slot-10Pole NWFSal FSM has achieved higher torque and power as compared to the 12Slot-8Pole OWFSal FSM as well as higher torque and efficiency when compared to the 12Slot-8Pole NWFSeg FSM. The power of the 12Slot-10Pole NWFSal FSM is still less than that of the NWFSeg FSM. To achieve better performance in terms of torque and power, the trapezoidal slots of the FEC and armature are transformed into rectangular slots for a smooth flow of flux as shown in Figure 13 and another three cycles of optimization are conducted to enhance the characteristics.

7. Performance analysis of optimized design

After updating various parameters using deterministic optimization techniques, the torque as well as the power of the NWFSal FSM are increased when compared to the refined design, as illustrated in Figure 14. The power accomplished after 3 cycles of optimization is 6.134 kW, while the torque achieved is 27.54 Nm. To achieve the target power, the number of turns is varied while fixing the applied armature and FEC current to find the optimum number of turns for the proposed design. Different turn combinations are evaluated, as shown in Figure 15, and the effects are highlighted on torque and power. From the graph, it is obvious that 44 turns have high average torque but less power. Similarly, at fewer turns, such as 37 and 38, much higher power is available due to less copper losses. Thirty-eight turns will be chosen for further investigation of efficiency of the optimized design as the target values of torque and power are achieved. The various parameters of initial design and optimized design are shown in Table 3. The number of turns of the armature windings is reduced

and the FEC and armature current have lower values, which will further boost the efficiency. Moreover, the slot area is reduced when compared to the initial and improved design, helping the flux to flow easily through the stator core.

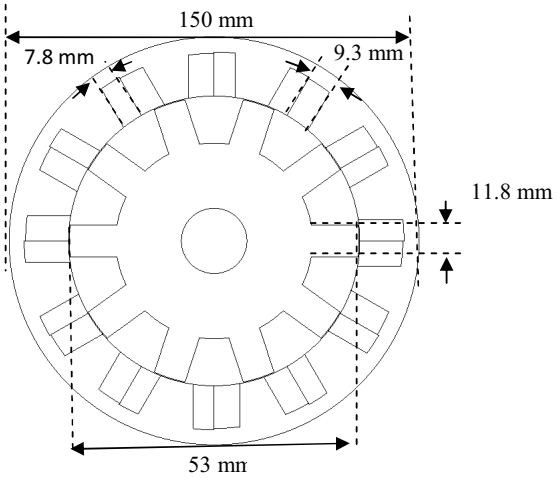

Figure 13. Optimized design of 12Slot-10Pole NWFSal FSM.

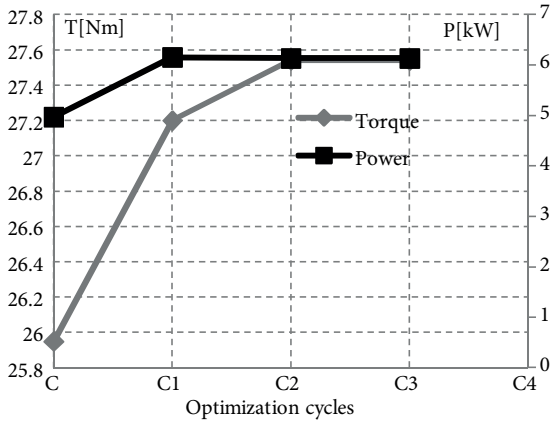

Figure 14. Optimization cycles to achieve better torque and power characteristics.

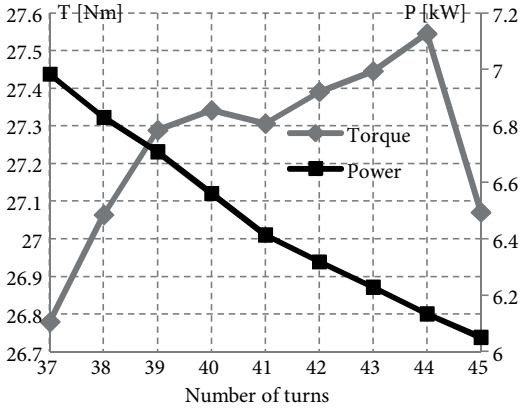

Figure 15. Torque and power versus number of turns.

Under no-load condition, the flux produced by the FEC of the optimized design at maximum J_e of 30 A/mm^2 is depicted in Figure 16. The flux produced by the optimized design has 20 times greater magnitude than the initial design. The torque and power versus armature current density, J_a, characteristics of the optimized design of the NWFSal FSM at maximum field current density, J_e, are plotted in Figure 17. From the graph, the linear increasing pattern of torque with respect to increase in J_a is observed. The maximum torque achieved by the optimized design is 27.06 Nm, which is 54% higher than the initial design, 4.6% higher than the NWFSeg FSM, and 52% higher than the OWFSal FSM. The proposed optimized design has achieved power of 6.83 kW at maximum J_a and J_e, which is higher than the OWFSal and NWFSeg FSMs. From the graph, it is noticeable that power decreases to lower amounts if J_a is applied beyond 25 A_{rms}/mm^2 due to copper loss, whereas the same phenomenon of power reduction is observed even at lower J_a values for the OWFSal and NWFSeg FSMs.

Table 3. Initial and optimized design parameters.

	Parameters	Initial	Optimized
R_1	Radius of rotor [mm]	45	53
R_2	Width of rotor [mm]	9.6	11.8
R_3	Depth of rotor [mm]	21	16
A_1	Armature slot width [mm]	13	7.8
A_2	Armature slot depth [mm]	21.7	16.33
F_1	FEC slot width [mm]	13	9.3
F_2	FEC slot depth [mm]	21.7	15.88
A_g	Length of air gap [mm]	0.3	0.3
S_a	Armature slot area [mm^2]	232.11	126.70
S_{fec}	FEC slot area [mm^2]	232.11	146.58
T	Average torque [Nm]	12.23	27.06
I_a	Armature current [A]	111.90	70.71
I_e	Field excitation current [A]	79.13	50
N_a	Armature turns	44	38
P	Power [kW]	3.12	6.83

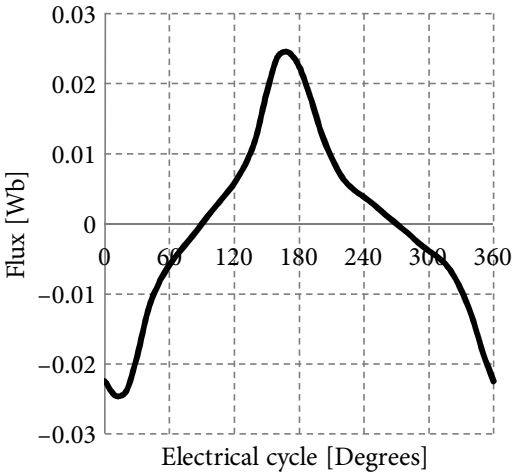

Figure 16. Flux linkage of optimized design.

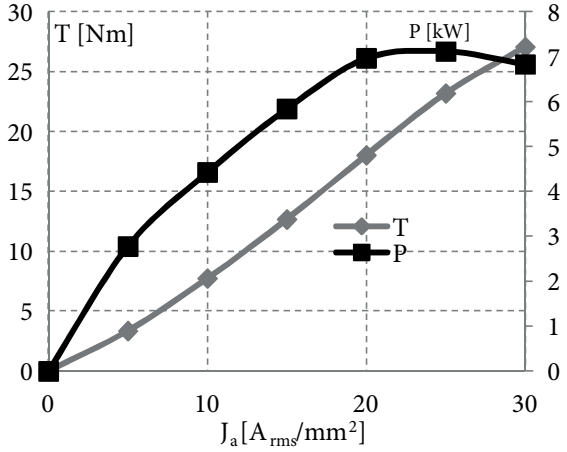

Figure 17. Torque and power vs. J_a at maximum J_e of 30 A/mm^2.

8. Conclusion

In this paper, design optimization and performance analysis of a new three-phase 12Slot-10Pole NWFSal FSM are presented and compared with 12Slot-8Pole OWFSal and NWFSeg FSMs. The novelty of the proposed design is nonoverlapping windings and salient rotor structure, which reduce the copper losses and make the rotor more robust. Although the initial design had insufficient torque and power production, the deterministic optimization approach adopted in this research has enhanced the torque, power, and efficiency compared to existing OWFSal and NWFSeg FSMs. The structure of the proposed machine is very simple, ensuring sufficient mechanical strength to operate at high speed. The JMAG designer registered version used as FEA software in this study has been confirmed by several papers as one providing good analytical accuracy. Consequently, it is realistic to assume that the simulation results shown in this paper are practicable. In conclusion, the analytical modeling and thermal study of this motor could be an attractive topic to investigate.

References

[1] Jahns T, Blasko V. Recent advances in power electronics technology for industrial and traction machine drives. P IEEE 2001; 89: 963-975.

[2] Bash M, Pekarek S, Sudhoff S, Whitmore J, Frantzen M. A comparison of permanent magnet and wound rotor synchronous machines for portable power generation. In: Power Energy Conference; 2010; USA. pp. 1-6.

[3] Sulaiman E, Kosaka T, Matsui N. Design and analysis of high-power/high-torque density dual excitation switched-flux machine for traction drive in HEVs. Renew Sust Energ Rev 2014; 34: 517-524.

[4] Chen Y, Zhu Z, Howe D, Ye Y. Starting torque of single-phase flux-switching permanent magnet motors. In: Proceedings of the IEEE International Magnetics Conference; 2006; San Diego, CA, USA. New York, NY, USA: IEEE. pp. 189-193.

[5] Sanabria-Walter C, Polinder H, Ferreira JA, Janker P, Hofmann M. Torque enhanced flux-switching PM machine for aerospace applications. In: Proceedings of the 20th International Conference on Electrical Machines; 2012; Marseille, France. New York, NY, USA: IEEE. pp. 2585-2595.

[6] Sung-Il K, Young-Kyoun K, Geun-Ho L, Jung-Pyo H. A novel rotor configuration and experimental verification of interior PM synchronous motor for high-speed applications. IEEE T Magn 2012; 48: 843-846.

[7] Miller TJE. Optimal design of switched reluctance motors. IEEE T Ind Electron 2002; 49: 15-27.

[8] Pollock C, Wallace M. The flux switching motor, a DC motor without magnets or brushes. In: Conference Record of the 1999 IEEE Industry Applications Conference; 1999. New York, NY, USA: IEEE. pp. 1980-1987.

[9] Tang Y, Paulides JJH, Motoasca TE, Lomonova EA. Flux-switching machine with DC excitation. IEEE T Magn 2012; 48: 3583-3586.

[10] Omar MF, Sulaiman E, Soomro HA. New topology of single-phase field excitation flux switching machine for high density air-condition with segmental rotor. Appl Mech Mater 2015; 695: 783-786.

[11] Khan F, Sulaiman E, Ahmad MZ. Coil test analysis of wound-field three-phase flux switching machine with non-overlapping winding and salient rotor. In: IEEE 8th International Power Engineering and Optimization Conference; 2014; Langkawi, Malaysia. New York, NY, USA: IEEE. pp. 243-247.

[12] Chen JT, Zhu ZQ, Iwasaki S, Deodhar R. Low cost flux-switching brushless AC machines. In: Proceedings of the IEEE Vehicle Power and Propulsion Conference; 2010; Lille, France. New York, NY, USA: IEEE. pp. 1-6.

[13] Sulaiman E, Teridi FM, Husin ZA, Ahmad MZ, Kosaka T. Performance comparison of 24S-10P and 24S-14P field excitation flux switching machine with single DC-coil polarity. In: Proceedings on the International Power Engineering & Optimization Conference; 2013; IEEE. pp. 46–51.

[14] Sulaiman E, Kosaka T, Matsui N. Design study and experimental analysis of wound field flux switching motor for HEV applications. In: 20th International Conference on Electrical Machines; 2012; Marseille, France. New York, NY, USA: IEEE. pp. 1269-1275.

[15] Mecrow BC, El-Kharashi EA, Finch JW, Jack AG. Segmental rotor switched reluctance motors with single-tooth windings. IEE P-Elect Pow Appl 2003; 150: 591-599.

[16] Zulu A, Mecrow BC, Armstrong M. Topologies for three-phase wound field segmented-rotor flux switching machines. In: 5th IET International Conference on Power Electronics, Machines and Drives; 2010; Brighton, UK. London, UK: IET. pp. 1-6.

[17] Pollock C, Pollock H, Brackley M. Electronically controlled flux switching motors: A comparison with an induction motor driving an axial fan. In: Conference Record of the IEEE IAS Annual Meeting; 2–6 November 2003. New York, NY, USA: IEEE. pp. 2465-2470.

[18] Pollock C, Pollock H, Barron R, Coles JR, Moule D, Court A, Sutton R. Flux-switching motors for automotive applications. IEEE T Ind Appl 2006; 42: 1177-1184.

[19] Pollock H, Pollock C, Walter RT, Gorti BV. Low cost, high power density, flux switching machines and drives for power tools. In: Conference Record of the IEEE IAS Annual Meeting; 2003. New York, NY, USA: IEEE. pp. 1451-1457.

[20] Zhou YJ, Zhu ZQ. Comparison of low-cost single-phase wound-field switched-flux machines. IEEE T Ind Appl 2014; 50: 3335-3345.

[21] Zulu A, Mecrow BC, Armstrong, M. A wound-field three-phase flux switching synchronous motor with all excitation sources on the stator. In: Energy Conversion Congress and Exposition; 2009; San Jose, CA, USA. New York, NY, USA: IEEE. pp. 1502-1509.